AIIM

Association for Information and Image Management

1100 Wayne Avenue, Suite 1100
Silver Spring, Maryland 20910

301/587-8202

Centimeter

Inches

MANUFACTURED TO AIIM STANDARDS
BY APPLIED IMAGE, INC.

1 of 1

FORMING OF SUPERPLASTIC CERAMICS

D.R. LESUER, J. WADSWORTH, and T.G. NIEH

Lawrence Livermore National Laboratory, P.O. Box 808, L-353, Livermore, CA 94550, USA*

Superplasticity in ceramics has now advanced to the stage that technologically viable superplastic deformation processing can be performed. In this paper, examples of superplastic forming and diffusion bonding of ceramic components are given. Recent work in biaxial gas-pressure forming of several ceramics is provided. These include yttria-stabilized, tetragonal zirconia (YTZP), a 20% alumina/YTZP composite, and silicon. In addition, the concurrent superplastic forming and diffusion bonding of a hybrid ceramic-metal structure are presented. These forming processes offer technological advantages of greater dimensional control and increased variety and complexity of shapes than is possible with conventional ceramic shaping technology.

1. INTRODUCTION

The forming of ceramics is generally difficult because the melting points of ceramics are relatively high and, consequently, the temperatures required to plastically deform ceramics are also high. The propensity for grain boundary separation in ceramics is also well-known. In the 1950s, extensive efforts were made in the western world and the former Soviet Union to hot fabricate ceramics using conventional metallurgical processes such as extrusion, rolling, and forging [1-4]. The goal was to produce near-net-shape parts in order to avoid expensive machining. A number of structural oxides, including CaO, MgO, SiO_2, ZrO_2, BeO, ThO_2, and Al_2O_3, were studied. As a result of this work, an improved understanding of ceramic deformation was developed but certain problems, and in particular the requirement for relatively high forming temperatures, still existed. For example, the temperature required for hot forging Al_2O_3 was found to be approximately 1900°C, which is extremely high from a practical standpoint. Subsequently, the concept of thermomechanical processing of ceramics was more-or-less abandoned.

Recent technical advances have changed this picture. First, advances in ceramic powder processing technology have greatly improved the quality of ceramic powders. High-purity ceramics of submicron grain size and more consistent microstructures are routinely prepared. Secondly, the observation that very fine-structure ceramic materials can exhibit superplastic behavior has led to an intensive study of fundamental issues affecting the deformation behavior of ceramic materials. As a result, the science of ceramic superplasticity is now well-advanced with issues such as grain size effects [5-7], the role of grain boundary impurities [8, 9], cavitation [10], concurrent grain growth

* This work was performed under the auspices of the U.S. Department of Energy by LLNL under contract No. W-7405-Eng-48. The financial support was provided by the Army Research Office.

[11-13], and elevated-temperature flow characteristics [14, 15] documented for a number of ceramic systems.

In addition many fine-grained polycrystalline ceramics have been demonstrated to be superplastic in tension. These include yttria-stabilized tetragonal zirconia polycrystal (Y-TZP) [14-18], Y-doped Al_2O_3 [19], Hydroxyapatite [20], β-spodumene glass ceramics [21, 22], and Al_2O_3-reinforced Y-TZP (Al_2O_3/YTZ) [23, 24], SiC-reinforced Si_3N_4 (SiC/Si_3N_4) [25], and iron-iron carbide (Fe/Fe_3C) [25] composites. The area of superplastic ceramics has been the subject of considerable interest and some review papers are now available. [26-28] The key characteristics of these materials are summarized in Table 1. It is worth noting that the grain sizes in most of the superplastic ceramics are less than 1 μm which is much smaller than those usually found in superplastic metals (< 10 μm). Because of the fineness of the microstructure, it is usually not thermally stable and grain growth, and in particular dynamic grain growth, during superplastic deformation of ceramics always occurred.

Improved understanding of these fundamental issues and the demonstration of superplasticity in a number of commercially attractive ceramics has increased attention in technological application of ceramic superplastic deformation. This paper presents examples of the superplastic forming of several ceramics. Recent work is described on biaxial gas-pressure forming of several commercially attractive ceramic materials, including YTZP, 20%Al_2O_3/YTZP, and silicon. In addition, we will present an example of the concurrent superplastic forming and diffusion bonding (SPF/DB) of a hybrid ceramic-metal (YTZP/C103) structure.

2 SUPERPLASTIC FORMING AND DIFFUSION BONDING

Several parts have been successfully formed superplastically from fine-grained 3Y-TZP. For example, Kellett et al. [29] demonstrated that submicron-sized (~0.23 μm) 3Y-TZP powders can be extruded superplastically, with an 8 to 1 reduction in area ratio (or a true strain of -2.2), at 1500°C to near full density. Panda *et al.* [30] and Yamana *et al.* [31] have applied a sinter-forging technique to form bulk ZrO_2 stabilized by various amount of Y_2O_3 from fine powders to full density at 1400°C. Recently, Wakai *et al.* [32] successfully formed a 3Y-TZP sheet sample at 1450°C in air using SiC tools; this is shown in Fig. 1. The superplastically formed parts have a smooth surface finish with great dimensional accuracy required for aerospace applications. Wu and Chen [33] further demonstrated that a 2Y-TZP containing 0.3 mol% CuO can be superplastically formed into hemispheric dome shapes at 1150°C, as shown in Fig. 2. This low temperature forming was a direct result of the decreasing melting point of the grain boundary glassy phase caused by the CuO addition, which was initially discovered by Kimura *et al.* [34] and Wakai *et al.* [35] The above advancement of reduction in forming temperature represents a major technological breakthrough for ceramic forming, because it eases the operation requirements for furnaces and tools. In the case of Al_2O_3, Carry and Mocellin [36] demonstrated bar bending and inverse extrusion of fine-grained Al_2O_3 at 1500 and 1600°C.

In the area of diffusion bonding, although concurrent superplastic forming and diffusion bonding (SPB/DB) have been used for metals, these two processes have not yet been incorporated into a single operation for ceramics. The only DB work was carried out by Nagano *et al.* [37-39] who successfully performed diffusion bonding between Al_2O_3/YTZ composites and 3Y-TZP at the superplastic temperatures, i.e., 1450-1550°C, for the parent materials. The bond strength was found to depend on the bonding temperature and the compositions of the parent materials (similar

and dissimilar). A maximum bond strength of greater than 1300 MPa was recorded in a 20%Al_2O_3/YTZ composite diffusion bonded at 1470°C [37].

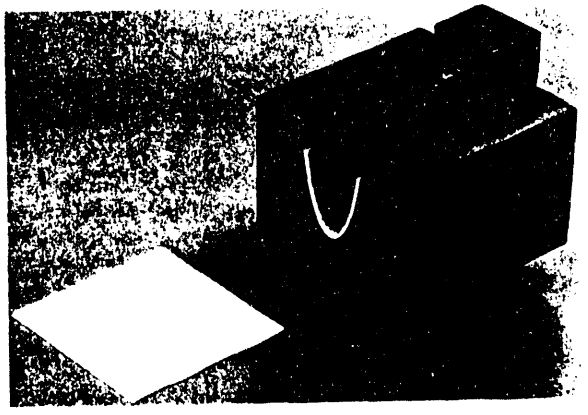

Fig. 1 Y-TZP sheet superplastically formed at 1450°C in air using SiC tools. (from Ref.[32])

Table 1 Property Data of Superplastic Ceramics and Ceramic Composites in Tension.

Material	Microstructure	Testing Parameters	Max. Elong., %	Material Variables	Ref.
Monolithics					
3Y-TZP	d = 0.3 μm		200	n = 2, p = 2, Q = 590 kJ/mol	[15]
3Y-TZP	d = 0.30 μm no glassy phase	1550°C 8.3×10^{-5} s^{-1}	800	n = 1.5, p = 3, Q = 510 kJ/mol	[14]
3Y-TZP	d = 0.3 μm	1450°C 4.8×10^{-5} s^{-1}	246	n = 2, p = NA, Q = 580 kJ/mol	[18]
Al_2O_3-500 ppm Y_2O_3	d = 0.66 μm	1450°C ~ 10^{-4} s^{-1}	> 65	n = NA, p/n = 1.5, Q = NA	[19]
Hydroxyapatite	d = 0.64 μm	1050°C 1.4×10^{-4} s^{-1}	> 150	n > 3, p/n = 1, Q = NA	[20]
β-spodumene glass	d = 0.91-2.0 μm >4 vol% galssy phase	1200°C 10^{-4} s^{-1}	> 400	n = 1, p = 3.1, Q = 707 kJ/mol	[22]
Composites					
20wt Al_2O_3/YTZP	d = 0.50 μm no glassy phase	1650°C 4×10^{-4} s^{-1}	620	n = 2, p = 1.5, Q = 380 kJ/mol	[40]
20wt Al_2O_3/YTZP	d = 0.50 μm	1450°C 10^{-4} s^{-1}	200	n = 2, p = NA, Q = 600 kJ/mol	[23]
10 vol% ZrO_2/Al_2O_3	d = 0.5 μm	1400°C 10^{-4} s^{-1}	>100	n = ?, p = ?, Q = ?	[41]
20wt% YTZP/Al_2O_3	d (ZrO_2) = 0.47 μm d (Al_2O_3) = 1.0 μm	1550°C 2.8×10^{-4} s^{-1}	110	n = 2, p = NA, Q = 700 kJ/mol	[42]
30wt% TiC/Al_2O_3	d = 1.2 μm	1550°C 1.2×10^{-4} s^{-1}	66	n = 4, p = NA, Q = 853 kJ/mol	[43]
β'-SiAlON	d = 0.4 μm with glassy phase	1550°C 10^{-4} s^{-1}	230	n = 1.5, p = NA, Q = NA	[44]
15 wt SiC/Si_3N_4	d = 0.2-0.5 μm with glassy phase	1600°C 4×10^{-5} s^{-1}	>150	n = 2, p = NA, Q = 649-698 kJ/mol	[25]
20 vol Fe/Fe_3C	d = 3.4 μm	1000°C 10^{-4} s^{-1}	600	n = 1.6, p = 2.9, Q = 200-240 kJ/mol	[45]

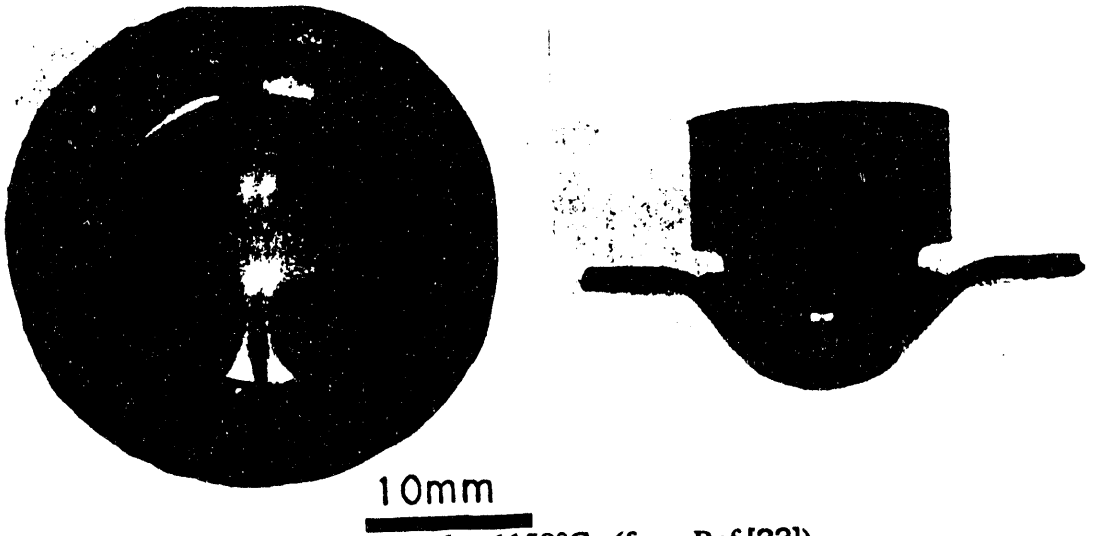

Fig. 2. Y-TZP sheet biaxially punch formed at 1150°C. (from Ref.[33])

3. GAS PRESSURE FORMING

3.1 Yttria-Stabilized, Tetragonal Zirconia Polycrystal (YTZP)

Specialized equipment was conceived, designed, and constructed to perform gas-pressure deformation of ceramic materials; this is described elsewhere [46]. Forming experiments were conducted over a temperature range of 1450° to 1600°C and forming pressures in the range of 345 to 2760 kPa. These forming temperatures and pressures were chosen to impart true strain rates over the range of approximately 10^{-5} to 10^{-2} s^{-1}. The forming behavior for YTZP sheet at a pressure of 690 kPa at various temperatures is summarized in the deformation-time plots of Fig. 3. Data in Fig. 3 exhibit three distinct regions of behavior as deformation progresses for each of the experimental conditions examined. Initially, the height of the deforming dome increases quite rapidly. This stage is followed by a period of apparent steady-state deformation. Finally, as the height approaches that of a hemisphere, the deformation rate increases again. The three-stage behavior shown in Fig. 3 appears to be similar to the creep curve of metal alloys deformed under a constant value of uniaxial stress. In this case, however, the interpretation is quite different.

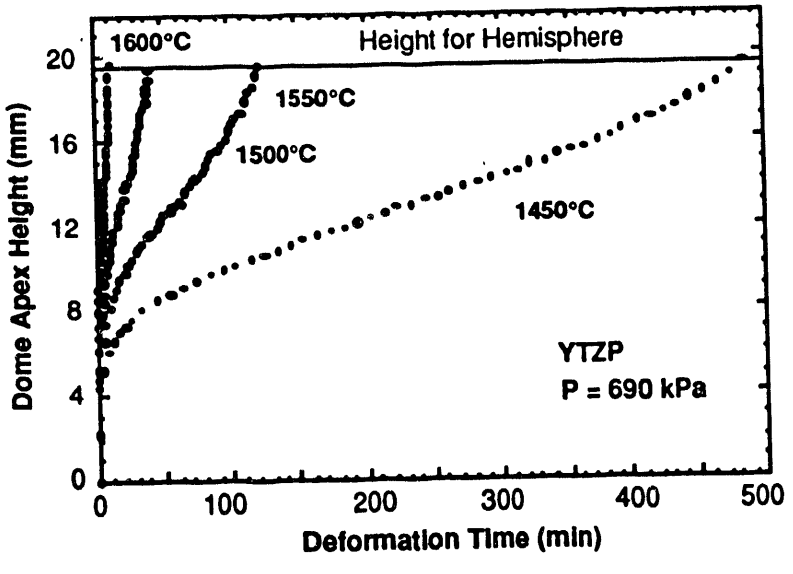

Fig. 3
Deformation-time curves for superplastic gas-pressure forming of YTZP.

Although the applied forming pressure remains constant throughout the test, the resultant stress acting in the deforming shell varies continuously during the course of deformation. The relationship between applied forming pressure and resultant shell stress can be explained through a consideration of the pressure-curvature relationship for a spherical shell:

$$\sigma = \frac{P\rho}{2t} \tag{1}$$

where σ is the principal tangential stress acting in a shell having a wall of thickness t and radius ρ, and P is the applied gas pressure. For the experiments of this study, P remains constant; ρ and t (and therefore σ) vary during the course of the test. Qualitatively, Eqn. (1) predicts a high flow stress σ at the beginning of a test (when the radius ρ is very high) and at the end of a test (as the thickness t decreases). The result of this variation in flow stress is a high forming rate at both low and high dome heights. As the thickness t and radius ρ are interdependent, the second stage of deformation occurs at an approximately constant rate because the decreasing radius of curvature is balanced by the decreasing shell thickness. Therefore, the three–stage behavior observed in Fig. 3 not only results from the creep of the material but also from the nature of constant–pressure biaxial forming.

For the testing conditions employed in this investigation, the relationship between flow stress and dome apex height has been calculated and is shown in Fig. 4. For discussion purposes, a nominal flow stress was selected for each of the forming pressures by averaging the curves shown in Fig. 4 for dome heights greater than 5 mm†. Note in Fig. 4 that for each forming pressure used, the predicted shell stress is closely approximated by a single nominal flow stress for a large portion of the test. This corresponds to the "steady-state" deformation (region 2) observed in the deformation-time plots presented in Fig. 3. The calculated results presented in Fig. 4 show that the imposed flow stress levels for the experiments of this study spanned the range of 3.75 MPa to 30 MPa. For each hemisphere formed, an average strain rate was calculated by simply dividing the final true apex thickness strain by the duration of the test. (It is clear that the strain rate changes continuously during the forming experiment for the constant forming pressure condition. The determination of average strain rate, therefore, provides only a first-order result.) In this manner, the forming stress–strain rate data are presented graphically as a log–log plot in Fig. 5. The data indicate that, at all temperatures, the average strain rate $\dot{\varepsilon}$, is proportional to the nominal flow stress raised to the nth power, i.e.:

$$\dot{\varepsilon} = B \cdot \sigma^{n} \tag{2}$$

The data of Fig. 5 exhibit a stress exponent n of 2 for the tests conducted at high applied pressure with n increasing to a value of 3 at lower applied stresses. A stress exponent of 3 in the low stress (or low strain rate) region is in agreement with results previously obtained from uniaxial tension tests (without compensating for dynamic grain growth during deformation) [17]. An increasing stress exponent in the low stress region has been observed previously in superplastic YTZP and was attributed to dynamic grain growth [14].

In the present study, concurrent grain growth occurs during superplastic biaxial deformation. For example, for the three hemispheres deformed at 1500°C at average strain rates of 1.65×10^{-4}, 1.29×10^{-3}, and 3.05×10^{-3} s^{-1}, the final grain sizes at the edge (representing static grain growth)

† The selection of the 5 mm height as a lower limit is justified by examination of Figure 3: deformation to a height of 5 mm occurs over a time which is brief compared to the total deformation time.

of the samples deformed at forming pressures of 690, 1380, and 2760 kPa were determined to be 0.28, 0.23, and 0.15 μm, respectively. Their corresponding grain sizes measured from the apex (representing the combined result of static and strain-enhanced grain growth) are 0.30, 0.24, and 0.20 μm, respectively. In comparison, the initial grain size was 0.15 μm. These results clearly show that for YTZP under balanced biaxial tension the kinetics of static grain growth (which represents just the influence of temperature) are significantly larger than the kinetics of strain-enhanced grain growth (which represents the influence of deformation). These results are consistent with the data of Yoshizawa and Sakuma [47] in which the kinetics of static and strain-enhanced grain growth were measured for YTZP in uniaxial compression.

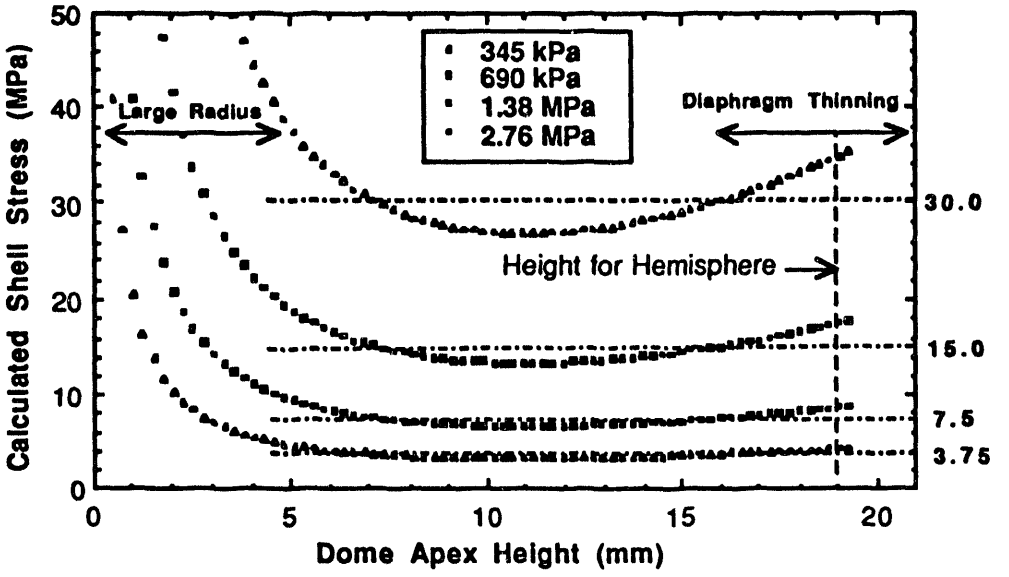

Fig. 4
Relationship between shell stress and dome apex height.

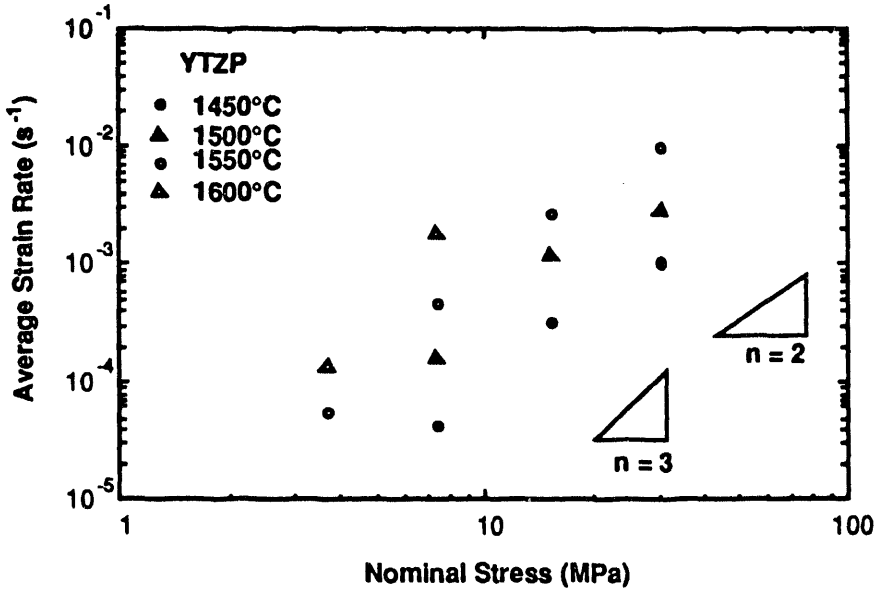

Fig. 5
Average strain rate versus nominal stress. Data indicate the stress exponent at low strain rates is about 3.

It is of interest to compare the present results at 1550°C with those from uniaxial tests. A direct comparison is shown in Fig. 6 between the strain rate–stress data obtained from the present biaxial forming experiments and those from uniaxial tests [14]. Data in Fig. 6 is plotted as average strain rate versus effective stress. It is evident in Fig. 6 that, despite the fact that the strain rate from the biaxial forming test is generally faster than that from the uniaxial tests, both sets of data indicate a slightly decreasing stress exponent in the high strain rate region.

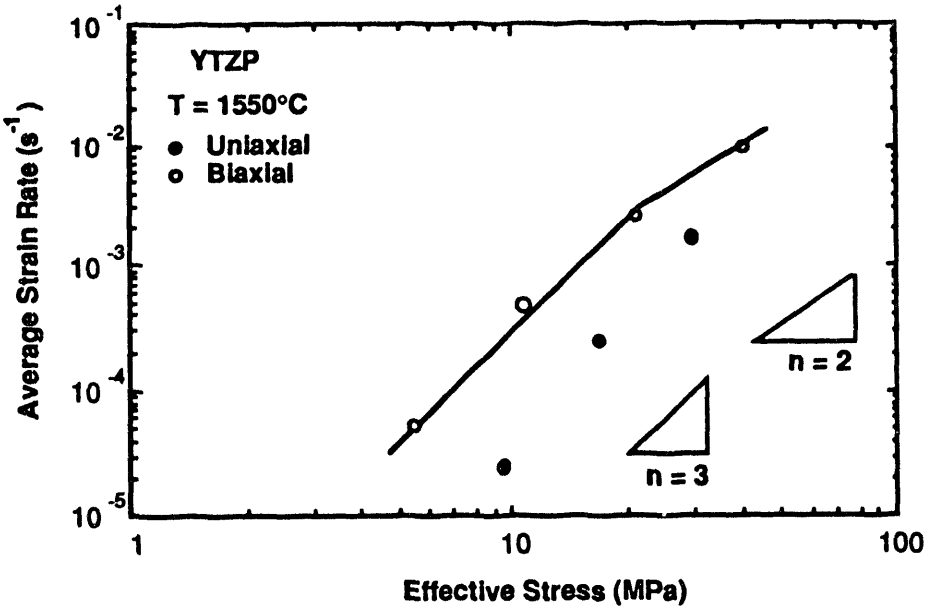

Fig. 6 A direct comparison between data from biaxial and uniaxial tests of YTZP.

The higher strain rate for the biaxial forming tests, versus the uniaxial tests, is believed to be caused primarily by uncertainty in the calculation of the nominal stress acting in the shell, eq. (1). Specifically, the uncertainty arises from the simplification of a nonuniform shell thickness during deformation. As a result of non-uniform thinning, the measured thickness at the apex of the formed hemispheres is much less than that predicted when a uniform thickness distribution is assumed. Concurrent dynamic grain growth may also contribute, in part, to the differences between the uniaxial and biaxial tests.

To assess the temperature dependence of the biaxial forming of YTZP, the activation energy, Q, was calculated from the data in Fig. 5. In Fig. 7, the activation energy is shown measured at a nominal stress of 10 MPa (in the $n = 3$ region). The value is determined to be about 530 kJ/mol which agrees well with the Q value of 580–590 kJ/mol obtained previously from uniaxial tests [15]. In summary, the stress and temperature dependences of strain rate (Figs. 5 and 7) obtained from biaxial tests are quite consistent with those obtained from uniaxial tests.

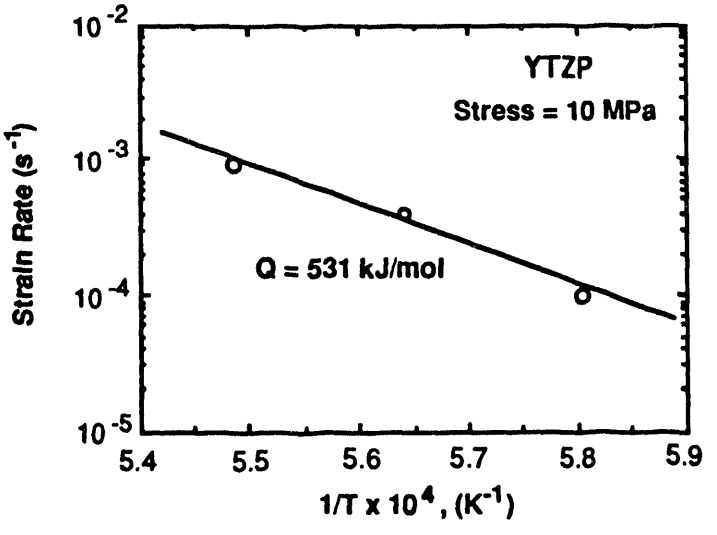

Fig. 7
An activation energy of about 531 kJ/mol is measured from the n = 3 region.

3.2 Alumina/YTZP

In the case of 20%Al_2O_3/YTZP, the hemispheres were deformed at temperatures between 1450 and 1600°C, and at forming pressures of 345 and 690 kPa. For the range of forming pressures and temperatures examined in this study, Al_2O_3/YTZP discs were deformed into hemispherical caps over times ranging from 10^3 to 2 x 10^4 s. The biaxial forming behavior for Al_2O_3/YTZP sheet is similar to that for YTZP. Namely, the forming curves essentially consist of three distinct regions. In a similar fashion, the nominal stress can be plotted as a function of average strain rate. The results indicate that the n value is approximately in the range from 2 to 3; n is 3 at 1500°C, but decreases to about 2 at 1550°C. These n values are in the usual range for superplastic ceramics. A comparison is shown in Fig. 8 between the strain rate-stress data obtained from biaxial forming of Al_2O_3/YTZP and data from uniaxial tests [40]. It is pointed out that the biaxial stress used in the figure is the tangential stress which equals $1/\sqrt{2}$ of the principal stress. Taking into account this factor, the strain rate from the biaxial forming test is about 3-4 times faster than that from the uniaxial tests; this result is similar to that found in YTZP.

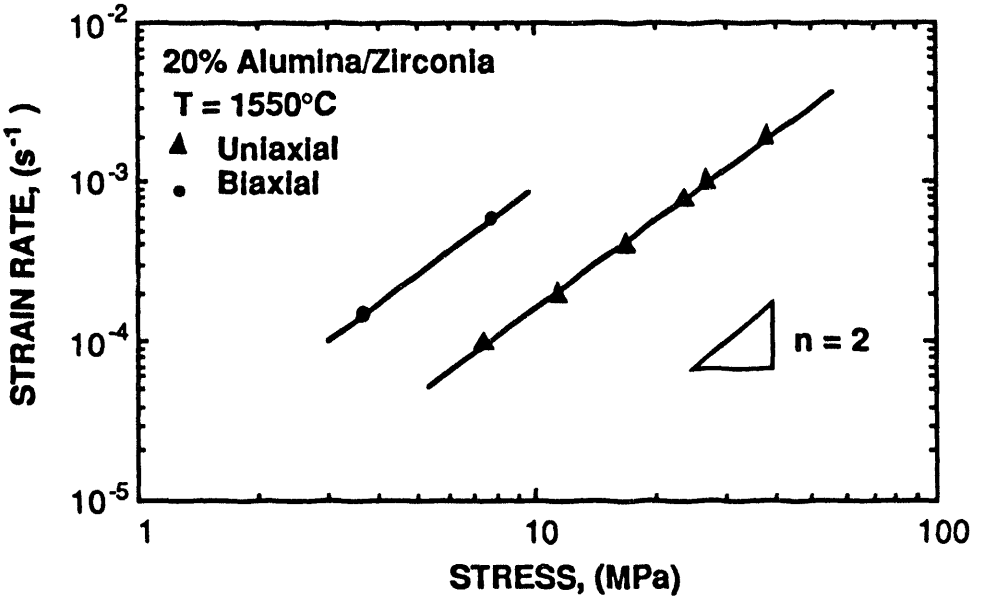

Fig. 8 Comparison between the strain rate-stress data obtained from the present biaxial forming experiments at 1550°C and those from uniaxial tests.

3.4 Silicon

Silicon is difficult to deform because of its diamond structure (covalent). Although some reported hot hardness data, indicated that Si softens at about 600-800°C, these data represent compression, not tension, properties of Si. The tensile ductility of Si becomes appreciable only at temperatures above 1300°C (melting point of Si is 1414°C) [48]. Net-shape forming of Si using casting techniques poses a major technical challenge because of strong chemical reactions between molten silicon and most crucible materials. In addition, Si virtually reduces the melting points of any chemical constituent. However, by proper selection of the mold material, the release agent for the mold, and the applied gas pressure, we have successfully formed single-crystal Si wafers into dome shapes [49]. A Si dome formed at 1375°C is shown in Fig. 9. This dome is noted to exhibit

a textured appearance, resulting from the constrained deformation of the single crystal. Such a texture can, presumably, be eliminated or reduced by replacing with a polycrystalline Si, in particular, fine-grained Si.

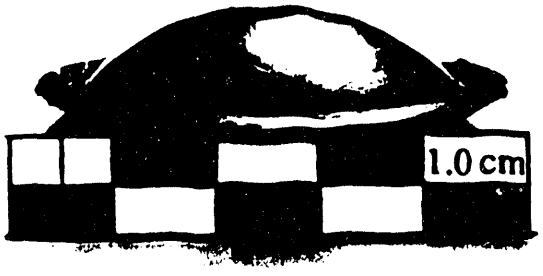

Fig. 9 A single-crystal Si dome formed at 1375°C.

4 HYBRID YTZP/C103 (SUPERPLASTIC FORMING AND DIFFUSION BONDING)

A combination of superplastic deformation with diffusion bonding offers the opportunity to manufacture a range of useful engineering structures. For example, ceramics can be bonded to metals during superplastic deformation to yield either a ceramic-metal laminate or to add selective metallization for attachment of fasteners. Further, individual ceramic sheets may be self–bonded during superplastic forming – allowing for the application of concepts such as fluids and integral cooling passages in net-shaped structures. High-temperature hardware may be manufactured which contains embedded sensors.

As an example of the potential for manufacturing metal-ceramic hybrids, the diffusion bonding and co-deformation of a YTZP ceramic disc and the Nb-based refractory alloy C-103 has been evaluated [50]. Alloy C-103 is a single-phase solid solution strengthened Nb alloy commonly used in spacecraft propulsion systems. Its nominal composition is Nb-10Hf-1Ti. Discs of YTZP and C-103 were assembled into the biaxial gas-pressure deformation apparatus and co-deformed at a temperature of 1500°C. Hemispherical sections with the Nb-based alloy integrally bonded to the underlying YTZP were successfully made. Thin-walled engineered metal-ceramic structures could have great utility in high thermal flux applications. Thus, the possibility to utilize superplastic deformation and simultaneous diffusion bonding creates the potential for the fabrication of truly unique engineering structures.

5. SUMMARY

In the past decade, ceramic superplasticity has rapidly advanced from a period of fundamental laboratory study to a level at which ceramic articles may be formed superplastically by gas pressure deformation. The next step in this evolutionary process is the actual manufacture of net-shaped articles. Using the technology developed for the present study, it is now possible to make intricately shaped, net shaped parts from superplastic ceramic sheet. Examples of such articles, a cone-on-cylinder geometry, a hat section, and a hemisphere are shown in Fig. 10. The articles were all formed within a forming time of 20 - 90 minutes (depending upon the strain required) at a forming pressure of 690kPa and a temperature of 1550°C. A multitude of shape geometries are possible with

this process – as determined by the shape of the die. Continued studies are needed to understand more fully the relationships between deformation variables (pressure, temperature) and deformation behavior (forming rate, strain distribution, cavitation).

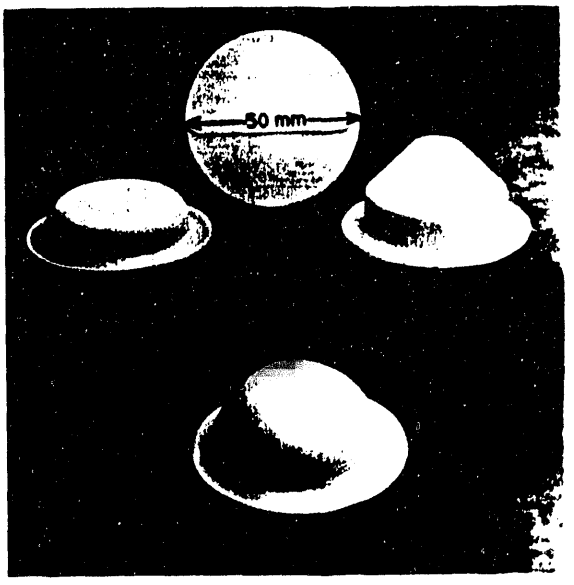

Fig. 10 Net-shaped articles superplastically formed from YTZP sheet are limited only by the die design.

REFERENCES

1. R.M. Fulrath: *Ceram. Bull.*, 1964, vol. 43,(12), pp. 880-885.

2. R.W. Rice: in *High Temperature Oxides, Chapter 3*, A.M. Alper eds., Academic Press, New York, 1970, pp. 235-280.

3. R.W. Rice: in *Ultrafine-Grain Ceramics*, J.J. Burke, N.L. Reed, and V. Weiss eds., Syracuse University Press, Syracuse, NY, 1970, pp. 203-250.

4. R.W. Rice: *J. Am. Ceram. Soc.*, 1993, vol. 76,(12), pp. 3009-3018.

5. T.G. Nieh and J. Wadsworth: *Scr. Metall. Mater.*, 1990, vol. 24, pp. 763-766.

6. T.G. Nieh and J. Wadsworth: *J. Mater. Res.*, 1990, vol. 5,(11), pp. 2613-2615.

7. F. Wakai and T. Nagano: *J. Mater. Sci.*, 1991, vol. 26, pp. 241-247.

8. T.G. Nieh and J. Wadsworth: *Scripta Metall.*, 1989, vol. 23, pp. 1261-1264.

9. Y. Ma and T.G. Langdon: in *Superplasticity in Metals, Ceramics, and Intermetallics, MRS Proceeding No. 196*, M.J. Mayo, J. Wadsworth, and M. Kobayashi eds., Materials Research Society, Pittsburgh, PA, 1990, pp. 325-330.

10. D.J. Schissler, A.H. Chokshi, T.G. Nieh, and J. Wadsworth: *Acta Metall. Mater.*, 1991, vol. 39,(12), pp. 3227-3236.

11. T.G. Nieh, C.M. Tomasello, and J. Wadsworth: in *Superplasticity in Metals, Ceramics, and Intermetallics, MRS Proceeding No. 196*, M.J. Mayo, J. Wadsworth, and M. Kobayashi eds., Materials Research Society, Pittsburgh, PA, 1990, pp. 343-348.

12. T.G. Nieh and J. Wadsworth: *J. Am. Ceram. Soc.*, 1989, vol. 72,(8), pp. 1469-1472.

13. F. Wakai, S. Sakaguchi, and H. Kato: *J. Ceram. Soc. Japan (In Japanese)*, 1986, vol. 94, pp. 72-75.

14. T.G. Nieh and J. Wadsworth: *Acta Metall. Mater.*, 1990, vol. 38, pp. 1121-1133.

15. F. Wakai, S. Sakaguchi, and Y. Matsuno: *Adv. Ceram. Mater.*, 1986, vol. 1, pp. 259-263.

16. F. Wakai, Y. Kodama, and T. Nagano: *Japan J. Appl. Phy. Series 2, Lattice Defects in Ceramics*, eds., Japan Journal of Applied Physics, Tokyo, Japan, 1989, pp. 57-67.

17. T.G. Nieh, C.M. McNally, and J. Wadsworth: *Scr. Metall.*, 1988, vol. 22, pp. 1297-1300.

18. T. Hermanson, K.P.D. Lagerlof, and G.L. Dunlop: in *Superplasticity and Superplastic Forming*, C.H. Hamilton and N.E. Paton eds., TMS, 1988, pp. 631-635.

19. P. Gruffel, P. Carry, and A. Mocellin: in *Science of Ceramics, Volume 14*, D. Taylor eds., The Institute of Ceramics, Shelton, Stoke-on-Trent, UK, 1987, pp. 587-592.

20. F. Wakai, Y. Kodama, S. Sakaguchi, and T. Nonami: *J. Am. Ceram. Soc*, 1990, vol. 73,(2), pp. 257-260.

21. J.-G. Wang and R. Raj: *J. Am. Ceram. Soc.*, 1984, vol. 67,(6), pp. 385-390.

22. J.-G. Wang and R. Raj: *J. Am. Ceram. Soc.*, 1984, vol. 67,(6), pp. 399-409.

23. F. Wakai and H. Kato: *Adv. Ceram. Mater.*, 1988, vol. 3,(1), pp. 71-76.

24. T.G. Nieh, C.M. McNally, and J. Wadsworth: *Scr. Metall.*, 1989, vol. 23, pp. 457-460.

25. F. Wakai, Y. Kodama, S. Sakaguchi, N. Murayama, K. Izaki, and K. Niihara: *Nature (London)*, 1990, vol. 334,(3), pp. 421-423.

26. T.G. Nieh, J. Wadsworth, and F. Wakai: *Inter. Mater. Rev.*, 1991, vol. 36,(4), pp. 146-161.

27. Y. Maehara and T.G. Langdon: *J. Mater. Sci.*, 1990, vol. 25, pp. 2275-2286.

28. I.-W. Chen and L.A. Xue: *J. Am. Ceram. Soc.*, 1990, vol. 73,(9), pp. 2585-2609.

29. B.J. Kellett, C. Carry, and A. Mocellin: in *Superplasticity and Superplastic Forming*, C.H. Hamilton and N.E. Paton eds., The Minerals, Metals, and Materials Society, Warrendale, PA, 1988, pp. 625-630.

30. P.C. Panda, J. Wang, and R. Raj: *J. Amer. Ceram. Soc.*, 1988, vol. 71, pp. C-507-C-509.

31. Y. Yamana, Y. Y., S. Nakamura, K. Kitagawa, T. Yoshimura, T. Mano, and Y. Shintani: *J. Ceram. Soc. Japan*, 1989, vol. 97, pp. 758.

32. F. Wakai: *Brit. Ceram. Trans. J.*, 1989, vol. 88, pp. 205-208.

33. X. Wu and I.W. Chen: *J. Am. Ceram. Soc.*, 1990, vol. 73,(3), pp. 746-749.

34. N. Kimura, H. Okamura, and J. Morishita: in *Advances in Ceramics, Vol. 24A*, S. Somiya, N. Yamamoto, and H. Yanagida eds., American Ceramic Society, Westerville, Ohio, 1988, pp. 183-191.

35. F. Wakai, H. Okamura, N. Kimura, and P.G.E. Descamps: in *Proc. 1st Japan Int'l SAMPE Symp.*, N. Igata, K. Kimpara, T. Kishi, E. Nakata, A. Okura, and T. Uryu eds., Society for the Advancement of Materials and Process Engineering, 1989, pp. 267-271.

36. C. Carry and A. Mocellin: in *High Tech Ceramics*, P. Vincenzini eds., Elsevier Science Publishers, Amsterdam, 1987, pp. 1043-1052.

37. T. Nagano, H. Kato, and F. Wakai: *J. Amer. Ceram. Soc.*, 1990, vol. 73,(11), pp. 3476-3480.

38. T. Nagano, H. Kato, and F. Wakai: *J. Mater. Sci.*, 1990, vol. 26, pp. 4985-4990.

39. T. Nagano and F. Wakai: in *MRS Intl. Meeting on Advanced Materials Vol 7 (IUMRS-ICAM-93, Symp. E-Superplasticity)*, M. Doyama, S. Somiya, and R.P.H. Chang eds., Pergamon Press, Netherland, 1993, pp. in press.

40. T.G. Nieh and J. Wadsworth: *Acta Metall. Mater.*, 1991, vol. 39, pp. 3037-3045.

41. L.A. Xue, X. Wu, and I.W. Chen: *J. Am. Ceram. Soc.*, 1991, vol. 74,(4), pp. 842-845.

42. F. Wakai, Y. Kodama, S. Sakaguchi, N. Murayama, H. Kato, and T. Nagano: in *MRS Intl. Meeting on Advanced Materials Vol 7 (IMAM-7, Superplasticity)*, M. Doyama, S. Somiya, and R.P.H. Chang eds., Materials Research Soc., Pittsburgh, Pennsylvania, 1989, pp. 259-266.

43. T. Nagano, H. Kato, and F. Wakai: *J. Am. Ceram. Soc.*, 1991, vol. 74,(9), pp. 2258-2262.

44. X. Wu and I.-W. Chen: *J. Am. Ceram. Soc.*, 1992, vol. 75,(10), pp. 2733-2741.

45. W.J. Kim, G. Frommeyer, O.A. Ruano, J.B. Wolfenstine, and O.D. Sherby: *Scr. Metall.*, 1989, vol. 23, pp. 1515-1520.

46. J.P. Wittenauer, T.G. Nieh, and J. Wadsworth: *J. Am. Ceram. Soc.*, 1993, vol. 76, pp. 1665-1672.

47. Y. Yoshizaka and T. Sakuma: *J. Am. Cera. Soc.*, 1990, vol. 73,(10), pp. 3069-3073.

48. D.W. Lillie: *Trans. TMS-AIME*, April 1956, vol. , pp. 249-251.

49. T.G. Nieh: LMSC-F070359, pp.7-301-7-321, Lockheed Missiles and Space Co., 1986.

50. J.P. Wittenauer, T.G. Nieh, and J. Wadsworth: in *Processing and Fabrication of Advanced Materials*, J.J. Morris eds., TMS, Warrendale, PA, 1992, pp. in press.

DATE
FILMED
9/29/94

END